applied sciences

MDPI

Article

Rainfall Variability and Droughts in the Sebou Basin (Morocco): ERA5 Bias Correction by Quantile Mapping and Trend Analysis over 1980–2024

Kawtar Rezkallah [1,*], Abdelali Sebbar [2], Pascal Maugis [3], Nir Y. Krakauer [4,5], Wahib Hammoudy [2] and Wadi Badri [1]

[1] Laboratory of Ecology and Environment (LEE), Faculty of Sciences Ben M'Sick, Hassan II University of Casablanca, Casablanca 20670, Moroccos
[2] General Directorate of Meteorology (DGM), Bd Mohamed Taïb Naciri, Hay Hassani, Casablanca 20200, Morocco; sebbar202@gmail.com (A.S.); hammoudy.wahib@marocmeteo.ma (W.H.)
[3] Laboratory for Climate and Environmental Sciences (LSCE), French Alternative Energies and Atomic Energy Commission (CEA), French National Centre for Scientific Research (CNRS), University of Versailles Saint-Quentin-en-Yvelines (UVSQ), Paris-Saclay,91191 Gif-sur-Yvette, France; pascal.maugis@lsce.ipsl.fr
[4] Earth and Environmental Sciences, The City University of New York Graduate Center, New York, NY 10016, USA; nkrakauer@ccny.cuny.edu
[5] Department of Civil Engineering, The City College of New York, New York, NY 10031, USA
* Correspondence: kawtarrezkellah@gmail.com

Abstract

Reconstructing long-term continuous precipitation series is essential for characterising rainfall variability, detecting hydroclimatic trends, and supporting water resource management in semi-arid Mediterranean regions. This study analyses rainfall variability in the Sebou watershed (northern Morocco, ~40,000 km^2) over 1980–2024, using eleven stations spanning an altitudinal gradient from 5 m (Kénitra) to 1478 m (Aït Khebbach). To reconstruct continuous monthly series over 44 hydrological years, ERA5 reanalyses were bias-corrected using seasonal Quantile Mapping (QM) versus station data, available only until 2001. Raw ERA5 data show a generalised positive bias increasing with altitude (from +8.9% at Kénitra to +112.9% at Pont du Mdez), with severe NSE degradation in complex relief areas (NSE = −3.834 at Pont du Sker). After QM correction, the mean bias drops to −0.1% and mean NSE improves from −0.32 to +0.68. Cross-validation (100 random-splitting iterations) confirms correction robustness, yielding a mean NSE of 0.594 ± 0.076. The stationarity hypothesis at the 2001/2002 boundary is validated for all eleven stations through the Pettitt test applied directly to the ERA5–OBS bias series (p = 1.000). Mann–Kendall trend analysis reveals no significant trend for most stations, reflecting strong natural decadal variability of the semi-arid Mediterranean regime, which may limit trend detection over the study period. SPI-12 analysis identifies four major drought episodes (1981–1985, 1991–1995, 1999–2002, 2018–2022) and notable wet surpluses (1995–1996, 2008–2010). Aïn Timédrine (650 m) shows notable chronic drought vulnerability (9 years with SPI-12 < −1.0). This study provides the first continuous 44-year monthly precipitation series for the Sebou basin, quantifies the ERA5 elevation mismatch (Δz) as the dominant bias predictor (r = −0.828, p = 0.002), and delivers a multi-scale drought characterisation (SPI-3, SPI-6, SPI-12), constituting a valuable dataset for long-term hydrological modelling.

Academic Editor: Nathan J. Moore

Received: 24 May 2026
Revised: 5 July 2026
Accepted: 10 July 2026
Published: 13 July 2026

 https://doi.org/10.3390/app16147023

Keywords: Sebou watershed; precipitation; ERA5; Quantile Mapping; Mann–Kendall; SPI; drought; Morocco

1. Introduction

Global warming has reached approximately 1.4 °C above pre-industrial levels [1,2], causing major alterations in precipitation distribution, a multiplication of prolonged drought episodes, and an intensification of extreme meteorological events worldwide [3,4]. The decade 2014–2023 is the hottest ever recorded [5], with these trends particularly pronounced in semi-arid and Mediterranean regions where hydrological vulnerability is already high [6–8].

Morocco, located in northwest Africa (21° N–37° N) at the confluence of Atlantic, Mediterranean and Saharan influences, is particularly sensitive to global warming [9,10]. Its climate, ranging from sub-humid in the north to arid in the south, is governed by large-scale atmospheric circulation patterns, notably the Azores High pressure system, Atlantic depressions, North Atlantic sea surface temperatures, West Mediterranean Oscillation (WEMO) and the Mediterranean Oscillation (MO) [9,11]. Observations over recent decades confirm a clear trend towards warming (+0.2 °C to +0.4 °C per decade since the 1960s) and decreasing rainfall (−3 to −30% depending on the region) [11,12], directly threatening rainfed agriculture, which constitutes the main source of income in rural areas [13,14].

The Sebou watershed, located in northern Morocco, is a strategic territory covering approximately 40,000 km². It is home to 1.8 million hectares of agricultural land and accounts for 60% of national olive oil production and 50% of sugar production [15,16]. Its strong dependence on rainfed agriculture makes it highly vulnerable to climate variability and change [17]. Recent studies show a significant decline in annual precipitation, reaching −30 to −50 mm per decade in the northern and eastern sectors of the basin, with marked winter and spring decreases on the Rif slopes [15]. Long-term projections anticipate significant reductions in river discharge in Moroccan northern basins under future climate scenarios [18,19].

Although several studies have evaluated ERA5 precipitation performance over Moroccan basins [20–22], revealing systematic biases that require correction, none has yet reconstructed a continuous monthly rainfall series over the Sebou basin spanning 1980–2024 using a seasonally calibrated Quantile Mapping function—a methodological gap that the present study addresses.

In this context, the present study is based on monthly rainfall data from eleven stations in the Sebou basin, held by the Agence du Bassin Hydraulique du Sebou (ABHS), covering an altitudinal gradient from 5 m (Kénitra) to 1478 m (Aït Khebbach). The observed data (1980–2001) are subjected to rigorous quality control including gap detection and filling, identification of outliers, and verification of series homogeneity. In order to extend the analysis over a longer period, ERA5 estimates are mobilised to complete the series over the period 2002–2024, enabling the availability of continuous series over 44 hydrological years. The biases of this reanalysis are significant and described by Hersbach et al. [23], making a preliminary evaluation of their relevance necessary. This study pursues three specific objectives: (i) How does altitude affect ERA5 precipitation error, and can seasonal Quantile Mapping eliminate topographic bias? (ii) Do long-term precipitation variations over 1980–2024 exhibit spatial heterogeneity across the Sebou basin? (iii) What are the characteristics of the major drought episodes using the Standardised Precipitation Index (SPI) analysis?

The remainder of the paper is organised as follows: Section 2 describes the study area; Section 3 presents the data and methodology; Section 4 reports the results; Section 5 dis-

https://doi.org/10.3390/app16147023

cusses the findings in the light of the existing literature; and Section 6 draws the main conclusions.

2. Study Area

The Sebou watershed, located in northern Morocco (between 32°30′–35°10′ N and 3°40′–6°55′ W), covers an area of approximately 40,000 km². It constitutes one of the most strategically important hydrological systems in Morocco, concentrating nearly 30% of national surface water resources and home to approximately 7.6 million inhabitants, representing 20% of the total population [16] (Figure 1).

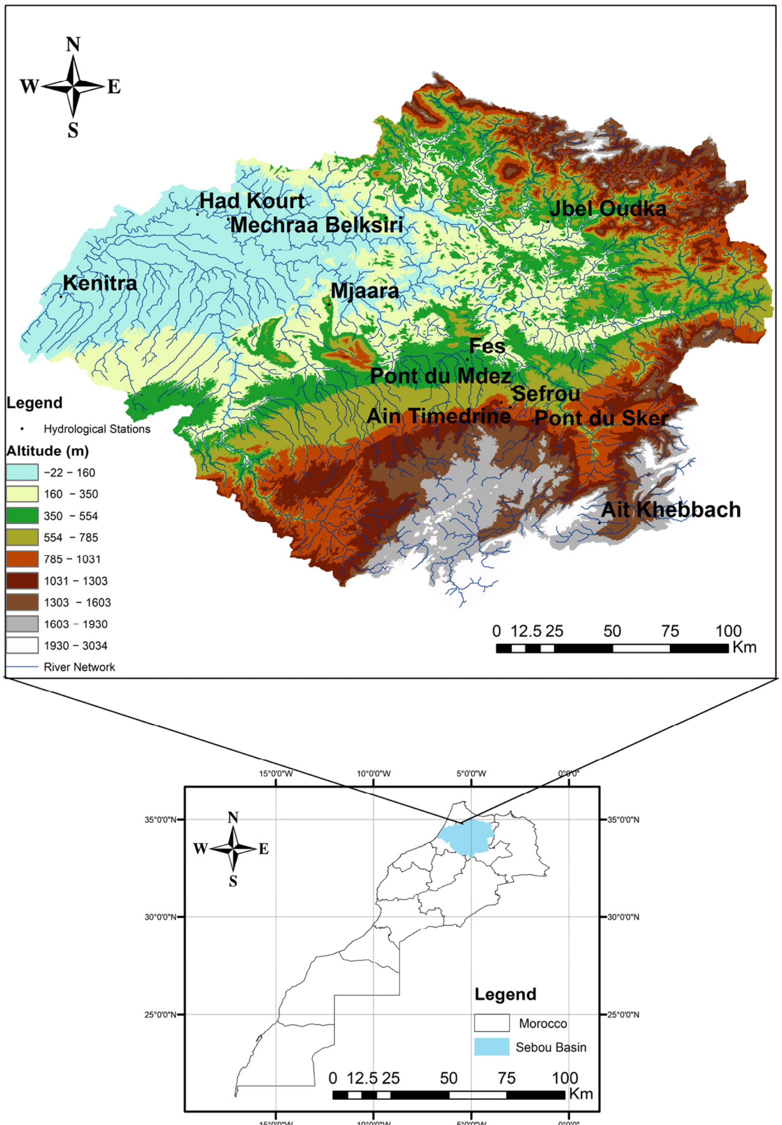

Figure 1. Location map of the study area.

Its relief is characterised by a strong altitudinal contrast, ranging from sea level at the Atlantic estuary (Kénitra) to 1478 m in the Middle Atlas at the highest gauging station (Aït Khebbach). It should be noted that the density of eleven stations over 40,000 km² represents a limitation of this study, inherent to the availability of long-term records in this semi-arid region. The basin exhibits a mean elevation of 650 m, an average slope of 8.7°, and a total topographic relief of 3357 m (ranging from −30 m at the Atlantic coast to 3327 m in the Middle Atlas massif). These topographic statistics were derived from the SRTM 1 arc-second (~30 m) Digital Elevation Model (SRTMGL1 V003), using spatial gradient analysis implemented in Python (version 3.13, rasterio and numpy libraries).

https://doi.org/10.3390/app16147023

This topography delineates three distinct morphological units: the coastal plains of the Gharb in the northwest, the Saïss plateau in the centre, and the Atlas massifs to the south and east. The hydrographic network is structured around the Oued Sebou, fed by its major tributaries: the Oued Ouergha (7300 km^2), the Oued Beht (9000 km^2) and the Oued Inaouène (3400 km^2) [16].

The climate, of Mediterranean type with semi-arid tendency, is characterised by strong seasonal rainfall, concentrated mainly between October and April. Annual totals show strong spatial variability, ranging from less than 400 mm in the lowland areas to more than 800 mm on the Rif and Middle Atlas reliefs [12,15]. Although eleven stations cannot fully represent the spatial heterogeneity of a 40,000 km^2 watershed, they span the full altitudinal gradient (5–1478 m) across the three main morphological units of the basin, thus sampling the main precipitation regimes for ERA5 and allowing for bias correction and hydroclimatic trend analysis.

3. Materials and Methods

3.1. Observed Data (OBS)

Monthly rainfall data, referred to as OBS, originate from the network of the Agence du Bassin Hydraulique du Sebou (ABHS) and cover the period 1980–2001 for the eleven representative stations of the Sebou watershed (Table 1). These time series were subjected to rigorous quality control, including the detection of outliers and homogeneity analysis.

To identify potential breaks in the series, the non-parametric Pettitt [24] and Buishand [25] tests were applied, complemented by a Monte Carlo approach to refine the detection of abrupt climatic breaks [26]. The results of the Monte Carlo simulations (n = 9999 iterations) are presented in Table 2. No statistically significant break ($p > 0.05$) was detected for any of the eleven stations, validating the homogeneity of the observed series over the period 1980–2001. Outlier detection was performed by flagging monthly precipitation values exceeding three standard deviations above the station climatological mean ($\mu + 3\sigma$). Among the 35 flagged values, cross-validation against neighbouring station records confirmed their physical consistency with documented intense Atlantic disturbances—notably the exceptionally wet episodes of January 1995 and December 1996, simultaneously recorded across multiple stations. All flagged values were consequently retained as genuine extreme precipitation events.

Table 1. Characteristics of the rainfall stations of the Sebou watershed.

Nº	Station	Nº Station	Province	Lat. (ºN)	Long (ºW)	Alt. (m)
1	Kénitra	4782	Kénitra	34.29	6.59	5
2	Mechraa Belksiri	5255	Sidi Kacem	34.56	5.96	15
3	Had Kourt	4104	Sidi Kacem	34.55	5.72	30
4	Mjaara	5128	Sidi Kacem	34.23	5.54	96
5	Pont du Sker	6288	Taounate	33.78	4.75	315
6	Fès	3817	Fès	34.06	5.01	415
7	Aïn Timédrine	576	Sefrou	33.85	4.87	650
8	Pont du Mdez	6248	Sefrou	33.67	4.52	725
9	Séfrou	6562	Sefrou	33.83	4.86	930
10	Jbel Oudka	4626	Taounate	34.55	4.69	1115
11	Aït Khebbach	748	Boulemane	33.42	4.78	1478

https://doi.org/10.3390/app16147023

Table 2. Monte Carlo simulation results (n = 9999)—break detection in the annual rainfall series of the 11 stations of the Sebou watershed (1980–2001).

Nº	Station	Alt. (m)	Break Year	Mean Before (mm)	Mean After (mm)	Δ (%)	Observed F	*p*-Value MC	Sig.
1	Kénitra	5	1994	478.7	599.1	+25.2	2.42	0.657	NO
2	Mechraa Belk-siri	15	1994	420.2	526.6	+25.3	2.29	0.683	NO
3	Had Kourt	30	1982	323.9	471.6	+45.6	1.73	0.825	NO
4	Mjaara	96	1994	492.8	617.2	+25.2	2.29	0.694	NO
5	Pont du Sker	315	1986	241.6	303.9	+25.8	4.25	0.359	NO
6	Fès	415	1997	395.0	262.4	−33.6	5.85	0.219	NO
7	Aïn Timédrine	650	1997	371.1	306.6	−17.4	1.74	0.824	NO
8	Pont du Mdez	725	1986	241.6	303.9	+25.8	4.25	0.352	NO
9	Séfrou	930	1997	484.9	352.1	−27.4	5.34	0.246	NO
10	Jbel Oudka	1115	1997	1471.6	1110.7	−24.5	1.75	0.807	NO
11	Aït Khebbach	1478	1987	280.2	371.0	+32.4	5.20	0.250	NO

Mean bef./aft. = mean annual rainfall before/after break (mm); Δ = relative change (%); F = Chow statistic; *p*-value MC = Monte Carlo (n = 9999); Sig. = $\alpha = 0.05$.

3.2. ERA5 Reanalyses

ERA5 reanalyses, produced by the European Centre for Medium-Range Weather Forecasts (ECMWF), were used to extend the precipitation series beyond the period of direct observation. ERA5 was selected over ERA5-Land as recent studies have shown no significant improvement in precipitation estimates for the latter over semi-arid Moroccan basins [22]. This product was selected for its well-documented performance in semi-arid Mediterranean regions [22,23] and its continuous temporal coverage spanning 1940 to the present.

ERA5 outputs provide global atmospheric estimates at a spatial resolution of 0.25° × 0.25° (approximately 28 km at Moroccan latitudes) and an hourly temporal resolution, aggregated here into monthly totals [23]. The extracted variable is total precipitation (total_precipitation), expressed in mm/month. Extraction was performed at the grid point nearest to each station. ERA5 geopotential data (variable z) were converted to geopotential height (z/g_0, $g_0 = 9.81$ m/s^2), used here as a first approximation of geometric altitude. The elevation difference Δz = Alt_station − Alt_ERA5 was computed for each of the eleven stations to quantify the mismatch between station elevation and ERA5 grid cell mean elevation. ERA5 outputs may exhibit orographic bias in areas of complex relief, due to the altitude difference between the observation site and the centroid of the reanalysis pixel, as well as the strong spatial variability of precipitation in such environments. This limitation is however mitigated by the subsequent application of the Quantile Mapping (QM) bias correction method. Technical processing of the data, downloaded in NetCDF format, was carried out under a Linux environment combining Climate Data Operators (CDO) and Python (cdsapi, xarray, netCDF4 and pandas libraries).

3.3. Evaluation of ERA5 Data Quality

Prior to any bias correction, the performance of ERA5 data was evaluated by direct comparison with station observations over the common reference period 1980–2001. This evaluation is based on the calculation of four statistical indicators for each of the eleven network stations. In addition, a correlation analysis between site altitude and these metrics was conducted, in order to quantify the influence of relief on the reliability of the reanalyses and to identify any biases related to the orographic effect on the spatial representativeness of the model.

(i) Pearson Correlation Coefficient (r)

The coefficient r measures the temporal synchronisation between ERA5 and observed series:

$$r = \frac{\sum_i \left(ERA5_i - \overline{ERA5}\right)\left(OBS_i - \overline{OBS}\right)}{\sqrt{\sum_i \left(ERA5_i - \overline{ERA5}\right)^2 \times \sum_i \left(OBS_i - \overline{OBS}\right)^2}} \tag{1}$$

thresholds retained are: $r \geq 0.85$ (good correlation), $0.60 \leq r < 0.85$ (acceptable), and $r < 0.60$ (weak) [27].

(ii) Root Mean Square Deviation (RMSD)

The RMSD is an average measure of the deviation between ERA5 and observations, expressed in mm.

$$\text{RMSD} = \sqrt{\frac{1}{n}\sum_{i=1}^{n}(ERA5_i - OBS_i)^2} \tag{2}$$

(iii) Relative Bias (RB)

The relative bias (%) quantifies the mean linear deviation between the two series.

$$\text{RB}(\%) = \frac{\overline{ERA5} - \overline{OBS}}{\overline{OBS}} \times 100 \tag{3}$$

A positive bias indicates an overestimation by ERA5, a negative bias an underestimation.

(iv) Nash–Sutcliffe Efficiency (NSE)

The NSE, widely used in hydrology, compares the sum of squared errors to the observation variance.

$$\text{NSE} = 1 - \frac{\sum_i (ERA5_i - OBS_i)^2}{\sum_i \left(OBS_i - \overline{OBS}\right)^2} \tag{4}$$

An NSE = 1 indicates a perfect fit. An NSE = 0 indicates that deviations and observations have the same variance, and NSE < 0 indicates poor performance.

3.4. Bias Correction by Quantile Mapping (QM)

Bias correction of ERA5 data was performed using the empirical Quantile Mapping (QM) method [28,29]. This approach was selected because it adjusts the full statistical distribution of ERA5 precipitation—including mean, variance, and quantiles to match observations [28,29], making it particularly well-suited for historical reanalysis bias correction in semi-arid regions where precipitation distributions are highly skewed. While methods such as Linear Scaling correct only the mean bias, and Quantile Delta Mapping (QDM) is specifically designed to preserve projected climate change signals in future projections [30], QM focuses on historical bias correction rather than future climate projection and is more appropriate for the present study.

This correction was applied separately for each of the four hydrological seasons (Autumn: OND; Winter: JFM; Spring: AMJ; Summer: JAS) and for each of the eleven stations, resulting in 44 distinct correction functions (11 stations × 4 seasons). The calibration period (1980–2001) yields 66 monthly values per season, whose adequacy is assessed empirically through the random-splitting cross-validation described in Section 3.5. Potential discontinuities at seasonal boundaries were verified on monthly totals and deemed negligible (<2 mm) given the monthly time step used.

The choice to apply this correction was maintained regardless of the level of temporal correlation observed. Indeed, the Pearson correlation coefficient (r) measures only the syn-

https://doi.org/10.3390/app16147023

chronisation of variability between series, whereas QM focuses on correcting the statistical distribution of values. These two dimensions being statistically independent, a station showing a high correlation coefficient may nevertheless display a significant systematic bias that QM can rectify. It should be noted that QM corrects the statistical distribution of ERA5 precipitation but cannot improve the temporal synchronisation between ERA5 and observed series. For stations with weak ERA5/OBS temporal correlation, the corrected series may exhibit improved distributional properties while retaining limited month-to-month temporal agreement. This structural limitation is discussed in Section 4.2 for the stations concerned. The method adjusts the cumulative distribution of ERA5 precipitation to that of observations according to the following function:

$$P_{corr} = {F_{obs}}^{-1}[F_{ERA5}(P_{ERA5})] \quad (5)$$

F_{ERA5} denotes the cumulative distribution function of ERA5 precipitation over the calibration period 1980–2001, and F^{-1}_{obs} the inverse of the cumulative distribution function of observations. For ERA5 values exceeding the observation range, linear extrapolation based on extreme quantiles was applied to preserve the statistical consistency of extreme events [31]. The robustness of the correction was evaluated by cross-validation using random splitting, consisting of randomly selecting 12 years out of 22 for validation, while QM parameters are fitted based only on the other 10 years of observations.

3.5. Validation of the Stationarity Hypothesis

The extension of the series over the period 2002–2024 rests on the hypothesis of stationarity of the relationship between ERA5 reanalyses and observations at the 2001 boundary. To investigate this characteristic, the temporal stability of the annual ERA5 series is verified over the entire period of 1980–2024 using the non-parametric Pettitt test [24]. This test ensures the absence of any structural break that could bias the data reconstruction. The test statistic is defined by:

$$U_t = \sum_{i=1}^{t} \sum_{j=t+1}^{T} sgn(X_j - X_i) \quad (6)$$

where sgn(x) = +1 if x > 0, 0 if x = 0, −1 if x < 0. The break point K = max|U_t| is significant if $p < 0.05$. The absence of a break at the 2001/2002 boundary lends credibility to the transfer of the QM function to 2002–2024 [28]. To more directly validate the stationarity of the ERA5/OBS relationship, the Pettitt test was additionally applied to the annual ERA5–OBS bias series over the calibration period (1980–2001). Results are presented in Section 4.3. More exhaustively, it would also be appropriate to verify the stationarity of the statistical characteristics of the series (rolling mean and variances), but this type of test requires them to be longer [32].

3.6. Reconstruction of Rainfall Series 1980–2024

The monthly rainfall series, reconstructed over the period 1980–2024, result from a hybrid approach combining ABHS observations (1980–2001) and ERA5 data corrected by the QM method (2002–2024). This methodology provides homogeneous continuity and statistical consistency at the junction of the two periods (2001/2002), thus avoiding break artefacts related to the change of data source.

The database thus constituted offers an uninterrupted series of 44 hydrological years, forming the basis for trend analysis and long-term climate variability in the Sebou basin.

3.7. Climate Trend Analysis

(i) Mann–Kendall Test (S)

The Mann–Kendall test [33,34] detects a significant monotonic trend.

$$S = \sum_{i=1}^{n-1} \sum_{j=i+1}^{n} sgn(X_j - X_i) \tag{7}$$

S > 0 indicates an upward trend, S < 0 a downward trend. The trend is significant if the *p*-value is below the chosen significance threshold of 0.05.

(ii) Sen's Slope (β)

The magnitude of the trend is quantified by Sen's slope [35].

$$\beta = median\left(\frac{X_j - X_i}{j - i}\right) forallj > i \tag{8}$$

The slope β is expressed in mm/year. A positive β indicates an increase in precipitation, a negative β a decrease.

3.8. Standardised Precipitation Index (SPI)

The Standardised Precipitation Index (SPI) was calculated in accordance with the methodology of McKee et al. [36] in order to characterise the severity and duration of drought episodes. The analysis focuses on three timescales: SPI-12 (annual), SPI-6 (semi-annual), and SPI-3 (seasonal), suited to the study of interannual variability and drought characterisation over the reconstructed period 1980–2024.

$$f(x) = \frac{x^{\alpha-1} \times e^{-x/\beta}}{\beta^{\alpha} \times \Gamma(\alpha)} \tag{9}$$

where $\alpha > 0$ is the shape parameter, β > 0 the scale parameter estimated by maximum likelihood, and $\Gamma(\alpha)$ the Gamma function. The fitted distribution is transformed into a standardised normal distribution to obtain the SPI. Classification follows the thresholds in Table 3.

Table 3. Classification of episodes according to SPI values [36].

SPI Value	Category
SPI ≥ 2.0	Extreme wet
1.5 ≤ SPI < 2.0	Severe wet
1.0 ≤ SPI < 1.5	Moderate wet
−1.0 < SPI < 1.0	Normal
−1.5 < SPI ≤ −1.0	Moderate drought
−2.0 < SPI ≤ −1.5	Severe drought
SPI ≤ −2.0	Extreme drought

4. Results

4.1. Characterisation of Raw ERA5 Data Performance

The evaluation of raw ERA5 data at a resolution of 0.25° × 0.25° against station data over the common period 1980–2001 reveals a generalised positive bias, indicating systematic overestimation of precipitation by ERA5. This bias varies considerably as a function of station altitude, highlighting the influence of orography.

The elevation differences Δz between station altitude and ERA5 grid cell mean elevation range from −398 m (Aïn Timédrine) to +147 m (Jbel Oudka), revealing a systematic over-representation of station altitude by ERA5 for 10 out of 11 stations (Table 4).

Table 4. Station elevation, ERA5 grid cell elevation, elevation difference (Δz), and raw ERA5 relative bias RB(%) for the eleven stations of the Sebou basin.

RB% (Before QM)	NSE (Before QM)	Δz (m)	Alt_ERA5 (m)	Alt_St (m)	Station
+8.9	0.831	−80	85	5	Kénitra
+23.9	0.803	−47	62	15	Mechraa Belksiri
+27.2	0.780	−90	120	30	Had Kourt
+56.4	0.441	−280	372	96	Mjaara
+107.9	−3.653	−290	605	315	Pont du Sker
+44.8	0.626	−162	562	415	Fès
+87.9	−0.453	−398	1040	650	Aïn Timédrine
+112.9	−1.659	−316	1041	725	Pont du Mdez
+45.1	0.237	−200	1040	930	Séfrou
−57.4	0.315	+147	968	1115	Jbel Oudka
+106.7	−1.426	−115	1593	1478	Aït Khebbach

A statistically significant negative correlation was found between Δz and RB(%) ($r = -0.828$, $p = 0.002$, $R^2 = 0.68$) (Table 5, Figure 2), while a bilinear regression incorporating both Δz and absolute station elevation yields a marginal improvement ($R^2 = 0.75$), revealing that the elevation mismatch is a strong predictor of ERA5 precipitation bias, rather than station altitude alone.

Table 5. Pearson correlation coefficients between ERA5 raw relative bias RB(%) and physiographic variables for the eleven stations of the Sebou basin. Δz = elevation difference between station altitude and ERA5 grid cell elevation. Significance threshold: $p < 0.05$.

Variable	r	*p*	Significance
RB% vs. Δz (m)	−0.828	0.002	Significant
RB% vs. Altitude (m)	0.151	0.658	Not significant
RB% vs. Distance to coast (km)	0.451	0.164	Not significant

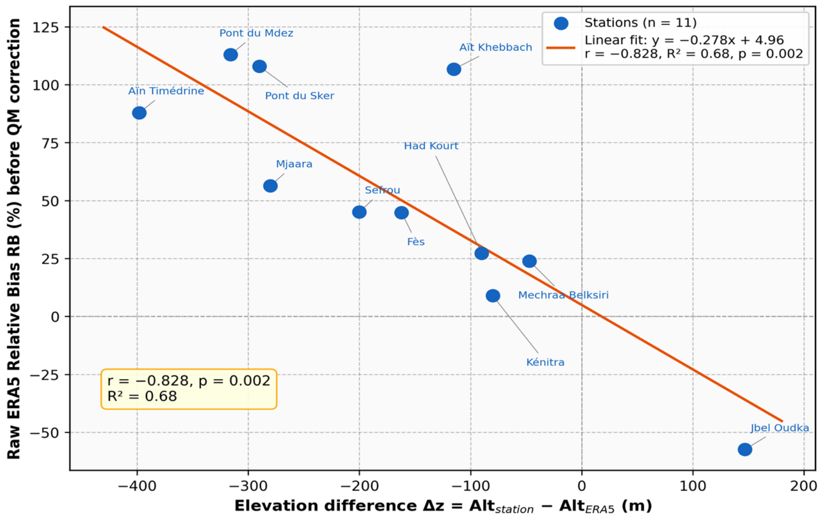

Figure 2. Relationship between ERA5-station elevation difference (Δz = Alt_station − Alt_ERA5) And raw ERA5 relative bias RB(%) for the eleven stations of the Sebou basin.

For low-altitude stations (z < 100 m), ERA5 estimates are globally satisfactory, confirming the good representativeness of ERA5 in the coastal plains of the Gharb (Table 4).

For intermediate-altitude stations (96–700 m), the bias roughly increases with elevation (Table 6, Figure 3). Pont du Sker constitutes a particular case: despite its moderate altitude, it exhibits the highest bias and the worst NSE in the network, primarily attributed to weak ERA5/OBS temporal synchronisation.

High-altitude stations (z > 700 m) present the most degraded performance (Table 7). Jbel Oudka constitutes a notable exception with a negative bias, suggesting an underestimation of ERA5 in this mountainous zone particularly exposed to Atlantic disturbances (Figure 3).

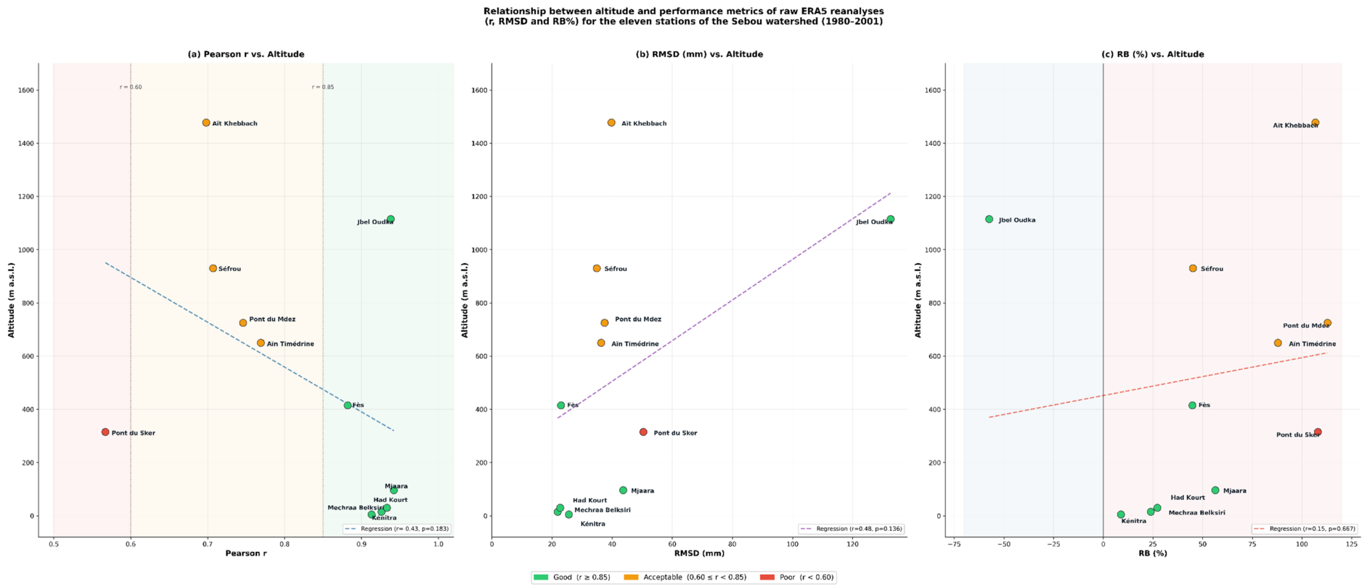

Figure 3. Relationship between altitude and performance metrics of raw ERA5 reanalyses (r, RMSD and RB%) for the eleven stations of the Sebou watershed (1980–2001).

Table 6. ERA5 performance metrics before and after QM correction for the 11 stations of the Sebou basin (1980–2001).

	Station	Alt (m)	r bef.	r aft.	Δr	RMSD Bef. (mm)	RMSD Aft. (mm)	ΔRMSD	RB Bef. (%)	RB Aft. (%)	NSE Bef.	NSE Aft.	ΔNSE
1	Kénitra	5	0.913	0.930	+0.017	25.6	23.2	−2.4	+8.9	−0.1	0.829	0.860	+0.031
2	Mechraa Belksiri	15	0.926	0.931	+0.005	21.9	18.2	−3.7	+23.9	−0.1	0.801	0.862	+0.061
3	Had Kourt	30	0.933	0.936	+0.003	22.7	17.2	−5.5	+27.2	−0.1	0.775	0.872	+0.097
4	Mjaara	96	0.942	0.947	+0.005	43.7	19.0	−24.7	+56.4	−0.1	0.438	0.894	+0.456
5	Pont du Sker	315	0.567	0.588	+0.021	50.4	20.8	−29.6	+107.9	−0.1	−3.834	0.175	+4.009
6	Fès	415	0.882	0.910	+0.028	23.0	15.9	−7.1	+44.8	−0.1	0.624	0.819	+0.195
7	Aïn Timédrine	650	0.769	0.796	+0.027	36.3	18.8	−17.6	+87.9	−0.3	−0.532	0.591	+1.123
8	Pont du Mdez	725	0.746	0.801	+0.055	37.5	14.5	−23.0	+112.9	−0.2	−1.675	0.600	+2.275
9	Séfrou	930	0.707	0.770	+0.063	34.9	26.9	−8.0	+45.1	−0.1	0.228	0.541	+0.313
10	Jbel Oudka	1115	0.938	0.956	+0.018	132.6	47.4	−85.2	−57.4	−0.1	0.311	0.912	+0.601
11	Aït Khebbach	1478	0.698	0.698	0.000	39.8	19.6	−20.2	+106.7	0.0	−1.485	0.396	+1.881

https://doi.org/10.3390/app16147023

Mean			0.820	0.842	+0.022	42.6	22.0	−20.6	+51.3%	−0.1%	−0.32	+0.684	+1.00

bef. = before QM correction; aft. = after QM correction; Alt = altitude.

Table 7. Cross-validation results by random splitting (100 iterations)—r, RMSD, RB(%) and NSE metrics before and after QM correction for the eleven stations of the Sebou watershed (1980–2001).

Nº	Station	Alt (m)	r	r	RMSD (mm)	RMSD (mm)	RB (%)	RB (%)	NSE	NSE
			Before QM	After QM	Before QM	After QM	Before QM	After QM	Before QM	After QM
1	Kénitra	5	0.90 ±0.02	0.85 ±0.02	25.4 ±2.4	32.1 ±6.8	9.0 ±3.1	−4.1 ±6.3	0.81 ±0.05	0.72 ±0.05
2	Mechraa Belksiri	15	0.92 ±0.01	0.88 ±0.01	21.7 ±1.6	23.4 ±3.0	25.1 ±4.4	−0.9 ±8.3	0.79 ±0.05	0.76 ±0.03
3	Had Kourt	30	0.93 ±0.01	0.89 ±0.02	22.6 ±2.2	22.2 ±3.0	27.2 ±3.4	−3.6 ±6.8	0.77 ±0.05	0.78 ±0.03
4	Mjaara	96	0.94 ±0.01	0.89 ±0.02	44.2 ±2.3	27.5 ±4.3	57.1 ±5.3	−2.1 ±8.5	0.42 ±0.12	0.78 ±0.03
5	Pont du Sker	315	0.57 ±0.03	0.59 ±0.03	50.7 ±3.7	21.0 ±1.8	109.9 ±9.2	2.0 ±9.0	−3.90 ±0.84	0.15 ±0.15
6	Fès	415	0.88 ±0.01	0.87 ±0.01	22.9 ±1.1	18.7 ±2.0	44.7 ±4.8	−2.6 ±8.6	0.62 ±0.05	0.74 ±0.02
7	Aïn Timé-drine	650	0.76 ±0.03	0.76 ±0.02	36.2 ±1.6	20.6 ±1.9	88.0 ±6.6	1.2 ±9.5	−0.55 ±0.20	0.49 ±0.11
8	Pont du Mdez	725	0.74 ±0.02	0.72 ±0.03	37.5 ±1.6	17.1 ±1.4	113.0 ±7.0	−0.1 ±7.8	−1.75 ±0.44	0.43 ±0.09
9	Séfrou	930	0.70 ±0.02	0.76 ±0.02	34.9 ±1.1	27.5 ±1.8	45.4 ±5.3	−0.5 ±9.8	0.21 ±0.09	0.50 ±0.07
10	Jbel Oudka	1115	0.93 ±0.01	0.92 ±0.01	132.4 ±11.2	63.4 ±8.9	−57.4 ±1.0	−2.2 ±5.6	0.30 ±0.01	0.84 ±0.02
11	Aït Kheb-bach	1478	0.69 ±0.03	0.67 ±0.05	39.8 ±1.7	20.6 ±1.7	108.0 ±9.8	1.3 ±11.3	−1.59 ±0.56	0.29 ±0.18

4.2. Performance and Robustness of Quantile Mapping Correction

Seasonal Quantile Mapping correction significantly reduces ERA5 RB(%) deviations for all eleven stations of the Sebou basin (Table 6, Figure 4). Among the 3036 monthly ERA5 values reconstructed over 2002–2024, only 7 (0.2%) fall outside the observation range and require linear extrapolation, thus inducing limited additional errors for these outlying values. After correction, RB(%) is reduced from +51.3% to −0.1%, and the mean NSE improves from −0.32 to +0.68. The correlation coefficient r remains globally stable after correction (variations below 0.06 according to Table 6), as QM adjusts the statistical distribution without modifying the temporal order of values, thus preserving the synchronisation between ERA5 and observations.

The greatest improvements are observed for stations with high initial RB(%). Pont du Sker records the largest improvement with ΔNSE = +4.009 (NSE: −3.834 → +0.175), followed by Pont du Mdez (ΔNSE = +2.275; NSE: −1.675 → +0.600) and Aïn Timédrine (ΔNSE = +1.123; NSE: −0.532 → +0.591). For low-altitude stations already well represented by ERA5, QM brings more moderate but consistent improvements: Had Kourt (ΔNSE = +0.097), Kénitra (ΔNSE = +0.031) and Mechraa Belksiri (ΔNSE = +0.061).

Jbel Oudka presents a particular case: with an initial negative RB(%) of −57.4%, QM corrects the ERA5 underestimation and produces the second-best performance after correction (NSE = 0.912), confirming the applicability of QM regardless of the sign of the initial RB(%).

Figure 4 visually illustrates these improvements: the Taylor diagram shows that all stations move closer to the OBS reference point after QM correction, with a simultaneous reduction in normalised standard deviation and centred RMSD, confirming a consistent improvement in the statistical representation of precipitation for all basin stations.

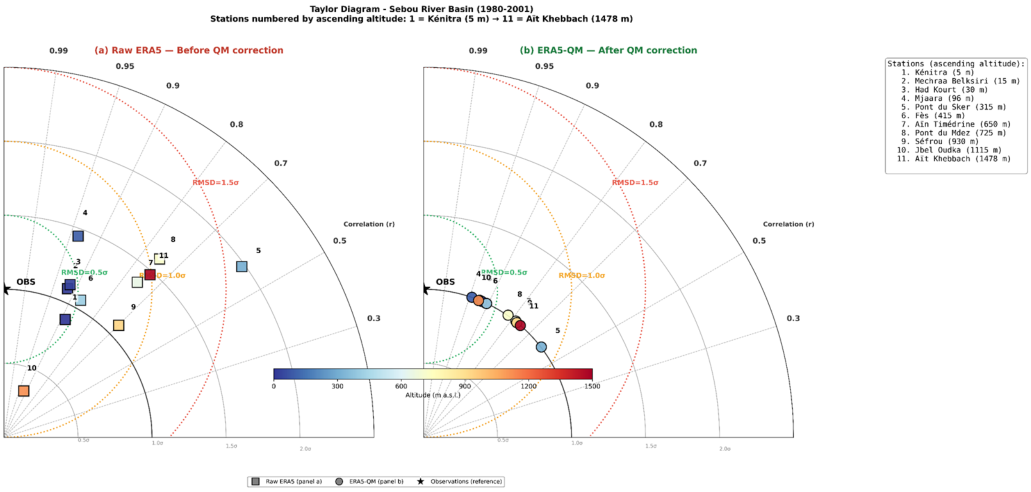

Figure 4. Taylor diagram comparing the performance of raw ERA5 reanalyses (panel (**a**), squares) and QM-corrected (panel (**b**), circles) for the 11 stations of the Sebou basin (1980–2001). Stations numbered 1 to 11 by increasing altitude (1 = Kénitra 5 m).

The robustness of the QM correction was evaluated by random splitting (100 iterations): at each iteration, 10 years are randomly drawn from the 22 available (1980–2001) for calibration, the remaining 12 years serving for independent validation [28].

Over the validation periods, the mean RB(%) is reduced from +51.8% to −1.1% ± 8.3%, the mean RMSD from 42.6 mm to 26.7 mm, the mean coefficient r remains stable (0.820 → 0.804), and mean NSE improves from −0.351 to +0.594 ± 0.076. A total of 9 out of 11 stations show an improvement in NSE after QM correction. For Kénitra and Mechraa Belksiri, the slight NSE degradation (ΔNSE = −0.093 and −0.027) is explained by the low initial ERA5 RB(%) for these lowland stations (Table 7, Figure 5).

The full distribution of NSE values across the 100 iterations (Figure 5) reveals that while most stations exhibit narrow interquartile ranges after QM correction, Pont du Sker (median NSE = 0.158), Pont du Mdez (median NSE = 0.43) and Aït Khebbach (median NSE = 0.367) show wider distributions, reflecting higher uncertainty at stations with weak ERA5/OBS temporal synchronisation.

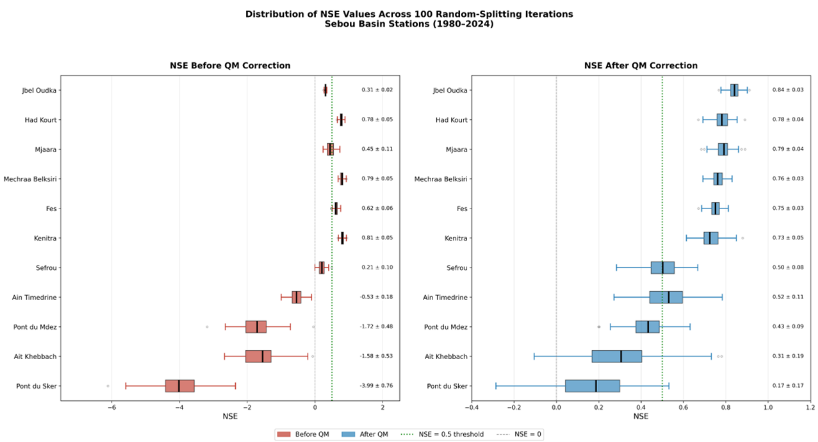

Figure 5. Distribution of NSE values across 100 random-splitting cross-validation iterations for the eleven stations of the Sebou basin, . Boxes represent the interquartile range (Q25–Q75), the vertical line indicates the median, and whiskers extend to Q10 and Q90. The green dashed line indicates the NSE = 0.5 threshold.

4.3. Validation of the Stationarity Hypothesis and Trend Analysis

The results of the stationarity and trend tests applied to the raw ERA5 series, station observations, and ERA5-QM series over the 1980–2024 period are presented in Table 8.

The Pettitt test detects no statistically significant breakpoint ($p < 0.05$) for any of the eleven stations, with all *p*-values equal to 1.0, confirming the absence of structural change in the series at the 2001/2002 boundary. Complementarily, the Pettitt test applied directly to the annual ERA5–OBS bias series over 1980–2001 also reveals no significant breakpoint at any station ($p = 1.000$), confirming that the bias characteristics—not merely the ERA5 series itself—remained stable throughout the calibration period. This strongly supports the stationarity assumption at the 2001/2002 boundary (Table 9).

The Mann–Kendall test applied to the annual ERA5 series detects no significant trend for ten stations ($p > 0.05$). Only the Aït Khebbach station (1478 m) shows a statistically significant downward trend at the 5% level ($Z = -2.20$, $p = 0.028$, Sen's slope = −1.55 mm/year). This trend is observed in the ERA5 series, but not in the station observations alone ($p = 0.06$).

This divergence suggests a potential temporal drift in ERA5 at this high-altitude station, which is eliminated by the QM correction (ERA5-QM: $p = 1.00$), confirming that bias correction can affect trend detection in reanalysis products. The *p*-value of 0.06 for the observed series approaches significance and may reflect limited statistical power over a 22-year record rather than a true absence of trend [37].

For the ten remaining stations, the stationarity assumption is validated, and from this perspective does not invalidate the transfer of the QM correction function to the 2002–2024 period.

Table 8. Results of stationarity tests (Pettitt and Mann–Kendall) applied to the annual ERA5 series (1980–2024).

Nº	Station	Alt (m)	Pettitt Break	Sig.	MK ERA5 1980–2024	MK ERA5-QM 1980–2024	MK OBS 1980–2001
1	Kénitra	5	2023	NO	NO ($Z = -1.30$, $p = 0.19$)	NO ($Z = -0.81$, $p = 0.42$)	NO ($Z = +0.40$, $p = 0.69$)
2	Mechraa Belksiri	15	2023	NO	NO ($Z = -1.30$, $p = 0.19$)	NO ($Z = -0.32$, $p = 0.75$)	NO ($Z = +0.85$, $p = 0.40$)
3	Had Kourt	30	2023	NO	NO ($Z = -0.87$, $p = 0.38$)	NO ($Z = -0.73$, $p = 0.46$)	NO ($Z = +0.17$, $p = 0.87$)
4	Mjaara	96	2023	NO	NO ($Z = -0.68$, $p = 0.50$)	NO ($Z = +0.03$, $p = 0.98$)	NO ($Z = +0.56$, $p = 0.57$)
5	Pont du Sker	315	2023	NO	NO ($Z = -0.66$, $p = 0.51$)	NO ($Z = +0.42$, $p = 0.67$)	NO ($Z = +1.35$, $p = 0.18$)
6	Fès	415	2023	NO	NO ($Z = -1.18$, $p = 0.24$)	NO ($Z = -0.85$, $p = 0.39$)	NO ($Z = -0.68$, $p = 0.50$)
7	Aïn Timédrine	650	2023	NO	NO ($Z = -1.93$, $p = 0.05$)	NO ($Z = -0.85$, $p = 0.39$)	NO ($Z = +0.79$, $p = 0.43$)

8	Pont du Mdez	725	2023	NO	NO (Z = −1.56, *p* = 0.12)	NO (Z = +0.19, *p* = 0.85)	NO (Z = +1.35, *p* = 0.18)
9	Séfrou	930	2023	NO	NO (Z = −1.93, *p* = 0.05)	NO (Z = −1.07, *p* = 0.29)	NO (Z = +0.11, *p* = 0.91)
10	Jbel Oudka	1115	2023	NO	NO (Z = −0.70, *p* = 0.49)	NO (Z = −0.25, *p* = 0.81)	NO (Z = −0.17, *p* = 0.87)
11	Aït Kheb-bach	1478	2017	NO	YES (Z = −2.20, *p* = 0.028) *	NO (Z = 0.00, *p* = 1.00)	NO (Z = +1.92, *p* = 0.06)

* Significant trend at the 5% level ($p < 0.05$).

Table 9. Pettitt test results applied to the annual ERA5–OBS bias series over the calibration period (1980–2001). Mean bias = mean annual ERA5–OBS difference; breakpoint year = year of maximum test statistic; *p*-value = significance of detected breakpoint; stable = no significant breakpoint detected ($p > 0.05$).

Stable	*p*-Value	Breakpoint Year	Bias Std (mm/yr)	Mean Bias (mm/yr)	Station
YES	1.000	1996	203.5	+52.2	Kenitra
YES	1.000	1996	176.8	+120.0	Mechraa_Belk-siri
YES	1.000	1996	177.7	+128.7	Had_Kourt
YES	1.000	1996	241.3	+308.3	Mjaara
YES	1.000	1995	196.0	−7.9	Pont du Sker
YES	1.000	1996	118.8	+171.5	Fès
YES	1.000	2001	135.0	+315.4	Ain Timedrine
YES	1.000	2001	121.9	+322.0	Pont du Mdez
YES	1.000	2001	134.6	+214.0	Séfrou
YES	1.000	1998	432.0	801.8	Jbel_Oudka
YES	1.000	2001	128.8	+361.7	Ait_Khebbach

Mean bias = mean annual ERA5–OBS difference (mm/yr); bias std = standard deviation of annual bias; breakpoint year = year of maximum test statistic; *p*-value = significance of detected breakpoint; stable = no significant breakpoint detected ($p > 0.05$).

4.4. Reconstructed Rainfall Series 1980–2024

The combination of ABHS station observations (1980–2001) and ERA5 data bias-corrected by QM (2002–2024) produces reconstructed monthly rainfall series spanning 44 hydrological years for the eleven stations of the Sebou basin. Potential seasonal boundary discontinuities related to QM were checked and deemed negligible (<2 mm on average), given the monthly time step used. The reconstructed series exhibit statistical continuity at the 2001/2002 boundary, with no breakpoint detected by the Pettitt test. Figure 6 illustrates annual rainfall trends for the eleven stations, revealing strong interannual variability characteristic of the semi-arid Mediterranean climate of the Sebou basin, with exceptionally wet years (1995–1996, 2008–2009) and prolonged drought episodes (1980–1985, 1999–2002, 2018–2022).

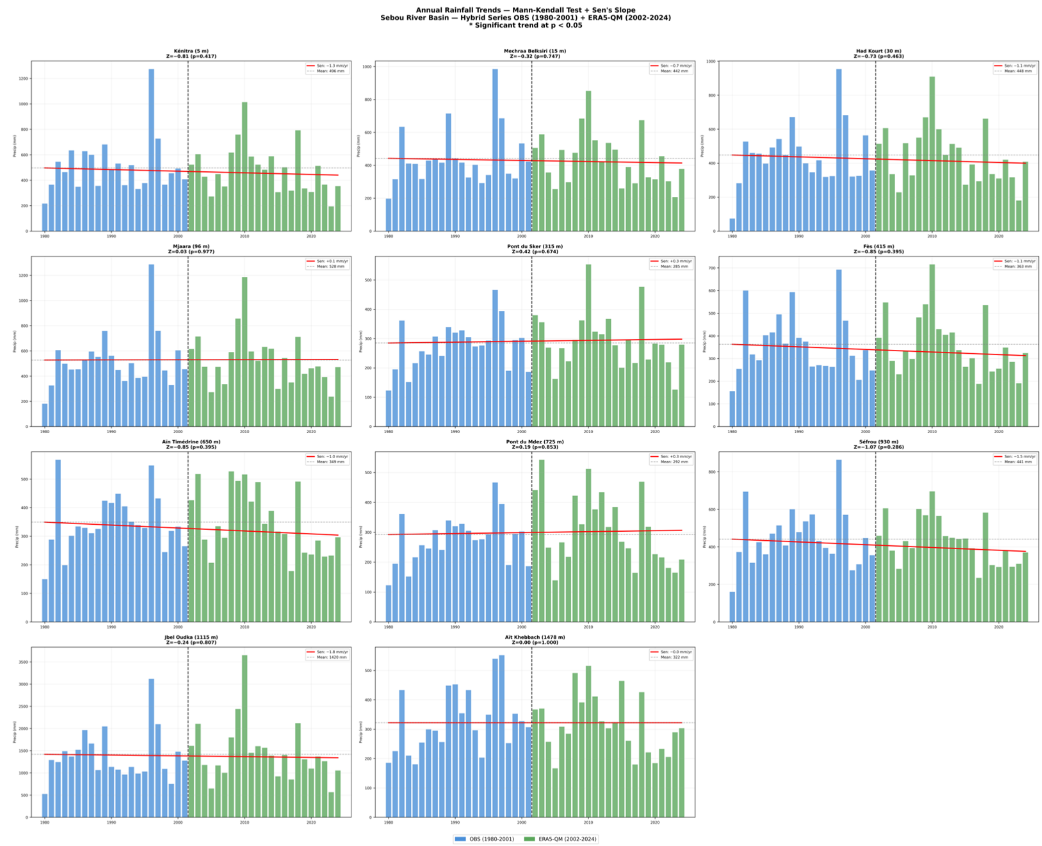

Figure 6. Annual rainfall trends (Sen's slope, mm/year) for the 11 stations of the Sebou basin (1980–2024). Blue and green bars represent the OBS (1980–2001) and bias-corrected ERA5-QM (2002–2024) series, respectively, separated by the vertical dashed line. The red line shows the Sen's slope trend and the grey dashed line the long-term mean.

4.5. Rainfall Variability and Drought Characterisation (SPI)

Analysis of the SPI-12 over the reconstructed 1980–2024 period reveals marked rainfall variability and alternating wet and dry episodes characteristic of the Sebou basin. Figure 7 presents the SPI-12 series for the eleven stations, enabling the identification of drought and water surplus episodes at the annual scale.

Several moderate-to-severe drought episodes (SPI ≤ −1.0) are consistently identified across all stations: 1981–1985, 1991–1995, 1999–2002, and 2018–2022. These periods coincide with the major droughts historically documented in Morocco [12,15,38]. Significant water surpluses (SPI ≥ +1.0) are observed for 1995–1996 and 2008–2010.

The four major drought episodes vary considerably in duration (17 to 27 months with SPI-12 ≤ −0.5) and severity (cumulative SPI-12 ranging from −16.1 to −35.6), with the 1991–1995 episode being the most severe and the 1999–2002 episode the longest (Table 10).

Among all stations, Aïn Timédrine (650 m) records the highest drought frequency with 9 years of annual mean SPI-12 < −1.0.

Spatial analysis of the SPI-12 reveals a degree of homogeneity in dry and wet episodes, although anomaly intensity is more pronounced in high-altitude areas (Aït Khebbach, Sefrou, Pont du Mdez), where winter precipitation associated with snowfall plays a predominant role.

Drought frequency is comparable across altitudinal zones (Figure 7), confirming the basin-wide character of drought dynamics. However, extreme drought events are more severe at high-altitude stations, with minimum SPI-12 values reaching −2.826 at Aït Khebbach (1478 m) compared to −2.791 at Kénitra (5 m).

At the half-yearly timescale (SPI-6, Figure 8), the four major drought episodes are consistently identified across all stations with sustained multi-month deficits, confirming their large-scale atmospheric origin. The 2018–2022 episode is the most persistent, with prolonged SPI-6 values below −1.0 at interior stations, indicative of a progressive moisture deficit driven by large-scale circulation anomalies.

At the seasonal timescale (SPI-3, Figure 9), precipitation variability is markedly amplified relative to longer timescales, reflecting the high intra-annual irregularity characteristic of semi-arid Mediterranean climates. Frequent alternations between wet and dry seasons are observed across all stations, with drought anomalies particularly pronounced at interior high-altitude stations (Aïn Timédrine, Pont du Mdez, Aït Khebbach), where seasonal precipitation deficits are structurally amplified by orographic effects.

Orographic effects tend to amplify seasonal precipitation deficits at interior high-altitude stations, though no systematic altitudinal gradient is observed at the annual timescale.

Table 10. Characterisation of major drought episodes over the Sebou River Basin based on basin-average SPI-12 (1980–2024). Duration: months with SPI-12 < −0.5; extent: maximum percentage of the eleven stations simultaneously recording SPI-12 ≤ −1.0 during the episode; severity: cumulative sum of negative SPI-12 values.

Episode	Duration (Months)	Max Areal Extent (%)	Min SPI-12	Severity
1981–1985	17	90.9	−1.50	−16.1
1991–1995	21	100.0	−2.29	−35.6
1999–2002	27	90.9	−1.91	−33.0
2018–2022	25	100.0	−1.58	−34.7

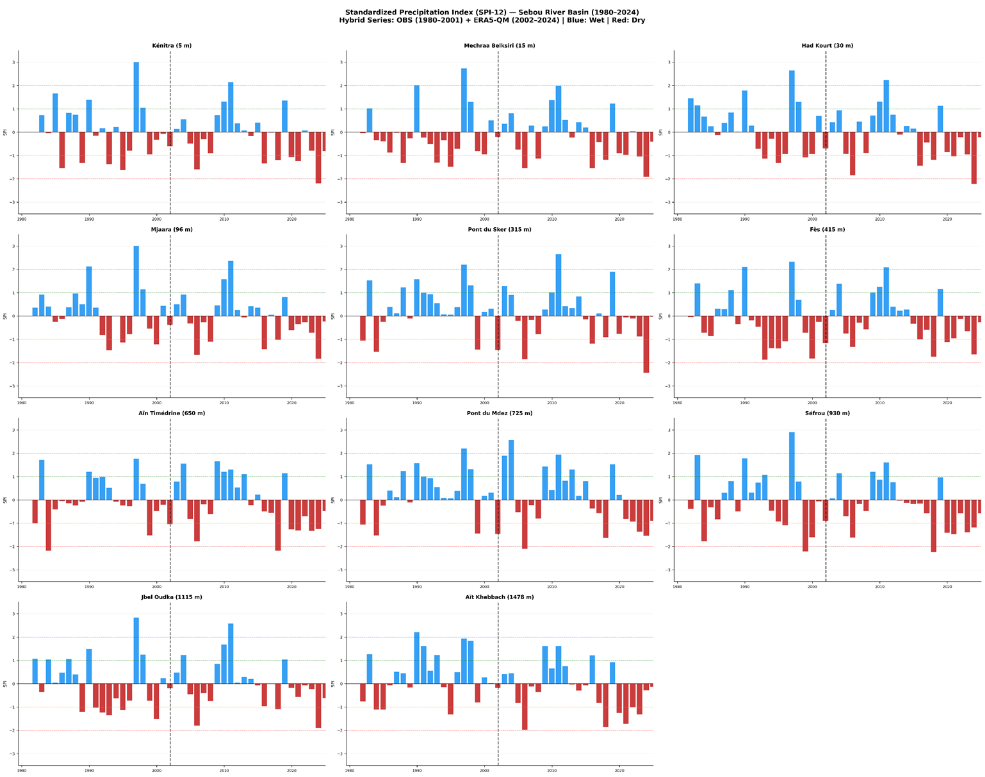

Figure 7. 12-month Standardised Precipitation Index (SPI-12) for the 11 stations of the Sebou basin (1980–2024). Blue bars indicate wet periods (SPI ≥ 0) and red bars indicate dry periods (SPI < 0). The

vertical dashed line marks the transition between the OBS (1980–2001) and bias-corrected ERA5-QM (2002–2024) series.

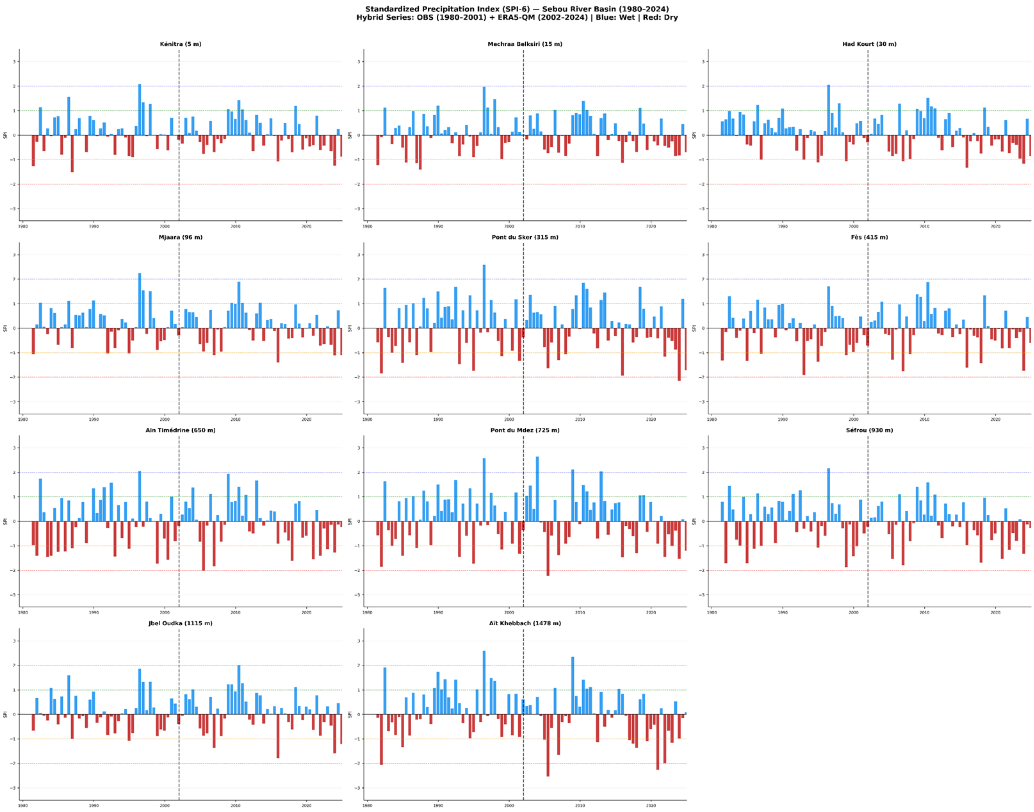

Figure 8. Standardised Precipitation Index at the medium-term scale (SPI-6) for the eleven stations of the Sebou basin (1980–2024), ordered by ascending altitude. Blue bars indicate wet periods (SPI-6 ≥ 0) and red bars indicate dry periods (SPI-6 < 0). Blue bars indicate wet periods (SPI ≥ 0) and red bars indicate dry periods (SPI < 0). The vertical dashed line marks the transition between the OBS (1980–2001) and bias-corrected ERA5-QM (2002–2024) series.

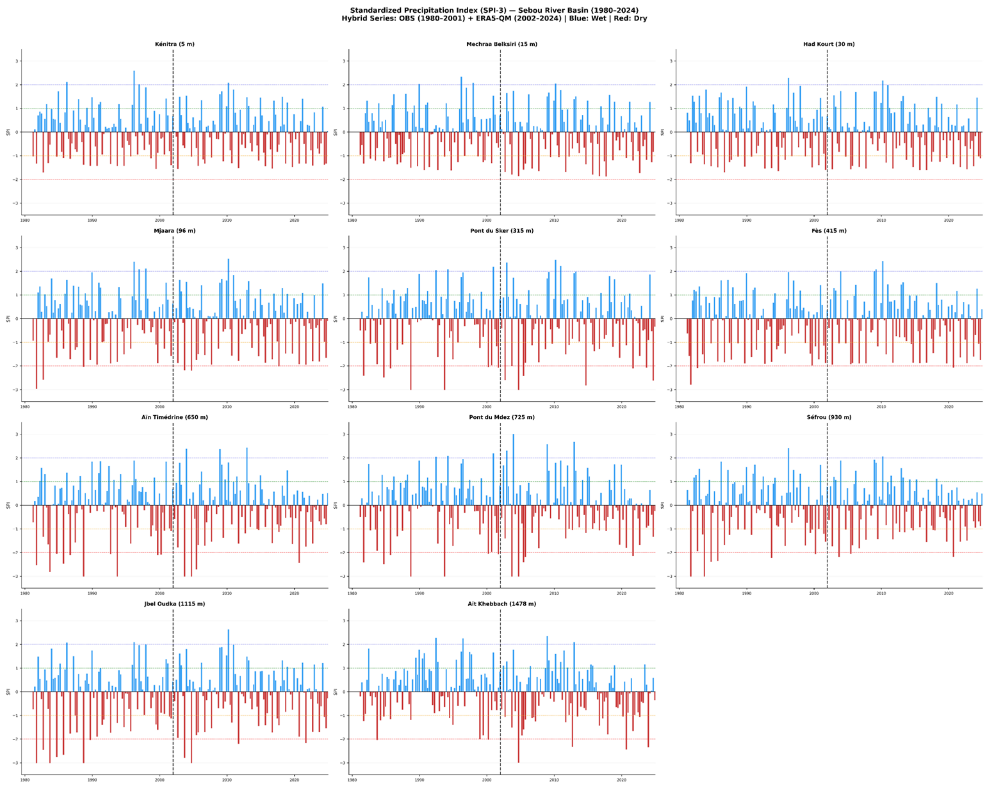

Figure 9. Standardised Precipitation Index at the seasonal scale (SPI-3) for the eleven stations of the Sebou basin (1980–2024), ordered by ascending altitude. Blue bars indicate wet seasons (SPI-3 ≥ 0) and red bars indicate dry seasons (SPI-3 < 0). Blue bars indicate wet periods (SPI ≥ 0) and red bars indicate dry periods (SPI < 0). The vertical dashed line marks the transition between the OBS (1980–2001) and bias-corrected ERA5-QM (2002–2024) series.

4.6. Basin-Wide Spatial Distribution of ERA5 Performance and Hydroclimatic Indicators

The four spatial indicators derived from the reconstructed 1980–2024 series are synthesised in Figure 10. The spatial distribution of ERA5 relative bias RB(%) (Figure 10a) confirms the dominant role of elevation mismatch Δz over station altitude as a predictor of ERA5 precipitation bias, as discussed in Section 4.1 (Tables 4 and 5). Post-correction NSE values (Figure 10b) reflect the dominant role of ERA5/OBS temporal synchronisation rather than altitude or geographic position, consistent with the analysis presented in Section 4.2. The spatial distribution of Sen's slopes (Figure 10c) confirms the absence of a discernible altitudinal or geographic gradient in precipitation trends across the basin, suggesting that trend dynamics are governed by large-scale atmospheric circulation patterns rather than local physiographic controls, as discussed in Section 4.3 [9,39]. Finally, SPI-12 drought frequency (Figure 10d) reveals a spatially homogeneous pattern across the basin, consistent with the large-scale character of the major drought episodes identified in Section 4.5.

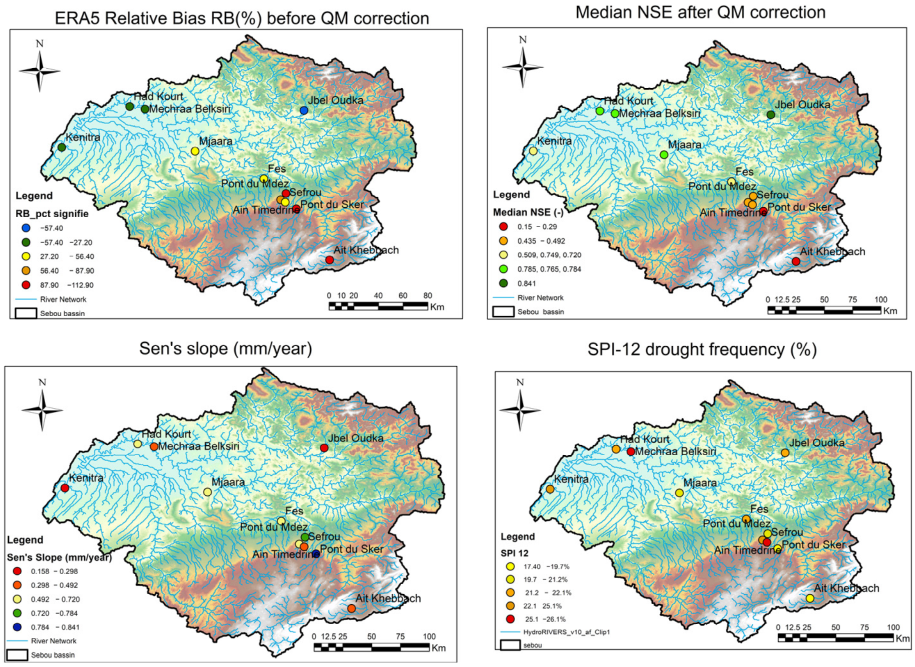

Figure 10. Spatial distribution of four hydroclimatic indicators across the eleven stations of the Sebou basin: (**a**) ERA5 raw relative bias RB(%) before QM correction; (**b**) Nash–Sutcliffe Efficiency (NSE) after QM correction; (**c**) Sen's slope (mm/year) from Mann–Kendall trend analysis (1980–2024); (**d**) SPI-12 drought frequency (% of years with annual mean SPI-12 ≤ −1.0).

5. Discussion

5.1. Homogeneity and Quality of Observed Data

Prior to any climate analysis, validating the homogeneity of observed rainfall series is a fundamental step. Monte Carlo simulations (n = 9999 iterations) applied to the eleven stations of the Sebou basin over the 1980–2001 period confirm the absence of any statistically significant breakpoint ($p > 0.05$) across the entire network (Table 2), consistent with the results of the Pettitt [24] and Buishand [25] tests. Potential detected breakpoints vary by station between 1982 (Had Kourt) and 1997 (Fès, Séfrou, Aïn Timédrine, Jbel Oudka), with p-values ranging from 0.219 to 0.825, all well above the threshold $\alpha = 0.05$. These results are consistent with the high natural variability of the semi-arid Mediterranean regime, in which interannual fluctuations can simulate apparent breakpoints without reflecting any real structural change in the series [26]. The robustness of this validation strengthens the reliability of the ABHS observations used as a reference for QM correction calibration over the 1980–2001 period.

5.2. ERA5 Bias Characterisation and Spatial Drivers

The systematic biases observed between ERA5 and station observations over the Sebou basin fall within a well-documented framework in the literature on global atmospheric reanalyses. ERA5's spatial resolution of 0.25°, although superior to previous generations, remains insufficient to faithfully capture the rainfall variability induced by the complex topography of the Middle Atlas and the Rif [40–42]. This finding aligns with Beck et al. [43], who, in an evaluation of 26 precipitation datasets over the contiguous United States (CONUS), show that ERA5 performs best in lowland regions but degrades significantly in semi-arid mountainous areas.

The tendency of ERA5 to overestimate precipitation at low- and mid-altitude stations (positive RB(%) for 10 out of 11 stations) is consistent with the findings of Jiang et al. [41] and Beck et al. [43], who show that ERA5 exhibits larger biases in areas of complex relief compared to plains. Low-altitude stations (z < 100 m) show the most satisfactory performance (RB(%) < 30%, r > 0.91, NSE > 0.77), confirming ERA5's good representativeness over the coastal plains of the Gharb, where homogeneous topography facilitates large-scale precipitation representation.

ERA5's underestimation at Jbel Oudka (RB(%) = −57.4%) reflects its unique geographical position at the interface between the Rif and Middle Atlas, where orographic lifting of Atlantic disturbances generates locally intense precipitation [9]. At 0.25° resolution, ERA5 is known to perform poorly in mountainous terrain [22], which likely explains the systematic underestimation observed at this station.

This result underscores that the ERA5/OBS discrepancy does not solely reflect model imperfections, but also within-grid cell heterogeneity: station observations may themselves not represent well the precipitation depth over the ERA5 grid cell extent, particularly in areas of complex relief [23]. A station-by-station approach is therefore warranted rather than a uniform regional correction.

5.3. Effectiveness and Robustness of Quantile Mapping Correction

The statistical non-significance of the RB(%) vs. altitude relationship (r = 0.24, p = 0.481, Figure 2) must be interpreted with caution: the exception of Jbel Oudka, with its atypical negative RB(%), disrupts the general upward trend.

The effectiveness of QM in the Sebou basin can be attributed to three key mechanisms. First, QM operates on the extensive cumulative distribution function, enabling simultaneous correction of mean bias, variance, and quantiles—a significant advantage in semi-arid regimes where precipitation distributions are highly skewed [28,29]. Second, the seasonal segmentation into four hydrological seasons captures the strong intra-annual variability characteristic of Mediterranean climates without introducing—here—transitional discontinuities, whilst a single transfer function would inadequately represent both wet winter and dry summer regimes [44]. Third, the empirical non-parametric implementation avoids misspecification errors inherent to parametric approaches when fitting theoretical distributions to highly skewed semi-arid precipitation series [29].

Furthermore, only seven out of 3036 reconstructed monthly values (0.2%) fall outside the calibration range, confirming that linear extrapolation remains marginal and does not significantly affect the quality of the reconstructed series.

The reduction in RB(%) from +51.3% to −0.1% over the calibration period (Table 6) demonstrates the remarkable effectiveness of QM in correcting systematic biases, regardless of their sign or magnitude. The case of Jbel Oudka is particularly instructive: starting from an initial negative RB(%) of −57.4%, QM yields the second-best post-correction NSE (0.912), confirming the method's universality. The stability of the correlation coefficient r after correction ($\Delta r < 0.065$ for all stations) suggests that QM adjusts for bias in the quantitative amounts without altering the temporal ordering of wet and dry periods, thereby preserving the synchronisation between ERA5 and observations [28,29].

The persistence of a modest NSE for Pont du Sker after correction (NSE = 0.175 despite RB(%) ≈ 0%) is explained by the low initial ERA5/OBS correlation (r = 0.567), a well-documented structural limitation: when temporal synchronisation is insufficient, correcting the statistical distribution alone cannot produce a high NSE [28,29]. This suggests that the spatial variability of precipitation at 315 m elevation in this area is too fine-grained to be captured by the ERA5 grid at 0.25°.

The robustness of the correction, assessed by random splitting over 100 iterations (Figure 5), confirms the transferability of the QM function to periods not used for calibration. The mean post-correction NSE over validation periods (0.594 ± 0.076) is in line with bias correction performance reported in the literature [28] for the correction of regional climate models.

The slight degradation in NSE after correction for Kénitra (ΔNSE = −0.093) and Mechraa Belksiri (ΔNSE = −0.027) warrants particular attention. These two low-altitude stations exhibit a low initial RB(%) (+9.0% and +25.1%, respectively), meaning that QM correction has limited room to improve the distribution without introducing minor temporal distortions. This phenomenon, known as "over-correction," has been documented by Lafon et al. [45] in their comparison of bias correction methods. Nevertheless, NSE values remaining above 0.72 for both stations indicate that their performance remains acceptable.

5.4. Stationarity and Trend Analysis

The absence of statistically significant breakpoints in the annual ERA5 series (Pettitt test, $p = 1.0$ for all stations except Aït Khebbach) validates the stationarity assumption of the ERA5/OBS relationship at the 2001/2002 boundary, a necessary condition for transferring the QM correction function to the 2002–2024 period. This absence of structural change further reinforces the validity of that transfer.

The marginally significant trend detected in the raw ERA5 series at Aït Khebbach (Z = −2.20, $p = 0.028$, slope = −1.55 mm/year) is absent from the ERA5-QM series ($p = 1.00$) as well as from station observations ($p = 0.06$). This divergence suggests that bias correction can be relevant to assessing the robustness of trends found in reanalysis products such as ERA5.

5.5. Drought Dynamics and SPI Analysis

The alternation of dry and wet episodes identified by the SPI-12 (Figure 7) is consistent with variability patterns of the North Atlantic Oscillation (NAO) and the Mediterranean Oscillation, which modulate rainfall inputs in Morocco at multi-year timescales [39]. The drought episodes identified (1981–1985, 1991–1995, 1999–2002, 2018–2022) coincide with the major droughts historically documented in Morocco [12,15,38], validating the consistency of the reconstructed series for climate variability analysis.

The 2018–2022 drought, particularly intense in the Sebou basin, is part of the aridification trend documented for the Mediterranean rim by Giorgi & Lionello [6], who project a winter precipitation reduction of approximately −20% in the southern Mediterranean under future climate scenarios. The absence of a significant trend over 1980–2024 for the majority of stations (Table 8) does not contradict these projections: the strong natural decadal variability of the Mediterranean regime makes declining trends statistically difficult to detect in series over the study period.

The notable chronic drought vulnerability of Aïn Timédrine (650 m, 9 years with SPI-12 < −1.0) can be explained by its location at the piedmont of the Middle Atlas at the transition between Atlantic-influenced plains and the continental interior. Precipitation at this station is primarily driven by Atlantic disturbances controlled by the Azores High. During positive NAO phases, the strengthening of the Azores High reduces Atlantic moisture penetration into the Moroccan interior, disproportionately affecting transitional stations such as Aïn Timédrine [9,11,39].

5.6. Limitations and Perspectives

The reconstructed rainfall series covering 1980–2024 constitute a valuable dataset for hydrological analysis of the Sebou basin, whose water resources are under increasing pressure from demographic growth and climate change [16]. Our results contribute to this dynamic and offer direct prospects for improving dam management models within the basin [16].

Several methodological limitations deserve mention. The stationarity of the ERA5/OBS relationship—the central assumption of the reconstruction—is verified only at the 2001/2002 boundary and could be called into question over longer future periods in the event of a structural shift in the climate regime [46]. Furthermore, the empirical QM used does not guarantee spatial consistency of the corrected series between stations, a limitation well-documented in the bias correction literature [47]. It should be noted that the Pettitt test detects abrupt changes in the mean but cannot formally exclude progressive changes in variance or distribution of the ERA5–OBS relationship beyond the calibration period. This represents an inherent limitation of the stationarity assumption, common to all reconstruction approaches based on historical calibration [46].

The SPI, based solely on precipitation accumulation, does not account for atmospheric water demand. In a context of rising temperatures documented across the Mediterranean region [6], the absence of evapotranspiration in the drought index may lead to an underestimation of drought severity, particularly during warm dry periods when evaporative demand amplifies water stress beyond what precipitation deficits alone can capture [48]. The Standardised Precipitation-Evapotranspiration Index (SPEI [48]), which incorporates the difference between precipitation and potential evapotranspiration, would provide a more comprehensive characterisation of drought under climate warming scenarios. Bias-corrected ERA5 temperature series—a natural extension of the present reconstruction—could serve as input for SPEI calculation, representing a direct avenue for future work, provided that stations are equipped with the necessary sensors to measure dew point temperature, air temperature and wind speed—variables required for potential evapotranspiration estimation—which may reduce the number of eligible stations or the length of available records.

6. Conclusions

This study reconstructed continuous monthly rainfall series spanning 44 hydrological years (1980–2024) for eleven stations of the Sebou watershed, by combining ABHS station observations (1980–2001) with ERA5 reanalyses bias-corrected through seasonal Quantile Mapping (2002–2024). ERA5 precipitation bias is primarily driven by the elevation mismatch Δz between station altitude and ERA5 grid cell elevation (r = −0.828, p = 0.002), rather than by station altitude alone.

Seasonal QM proved highly effective, reducing mean bias to −0.1% and improving mean NSE from −0.32 to +0.68, with robustness confirmed by cross-validation (mean NSE = 0.594 ± 0.076). Trend analysis revealed no significant rainfall trend for the majority of stations, consistent with the strong natural decadal variability of the semi-arid Mediterranean regime, which may limit trend detection over the study period. SPI analysis identified four major drought episodes (1981–1985, 1991–1995, 1999–2002, 2018–2022), with Aïn Timédrine exhibiting the highest chronic drought vulnerability. The reconstructed series constitute a robust dataset for hydrological modelling and water resource planning in the Sebou basin.

Author Contributions: Conceptualisation, K.R. and A.S.; methodology, K.R. and W.H.; software, K.R.; validation, K.R. and W.B.; formal analysis, P.M.; investigation, N.Y.K.; resources, A.S.; data curation, A.S.; writing—original draft preparation, K.R.; writing—review and editing, P.M. and N.Y.K.; visualisation, K.R.; supervision, W.B. and A.S.; project administration, A.S. All authors have read and agreed to the published version of the manuscript.

Funding: This research received no external funding.

Institutional Review Board Statement: Not applicable.

Informed Consent Statement: Not applicable.

Data Availability Statement: Data are available upon reasonable request from the corresponding author. ERA5 reanalysis data are openly available at https://cds.climate.copernicus.eu (accessed on 14 April 2025).

Acknowledgments: The authors would like to thank the Agence du Bassin Hydraulique du Sebou (ABHS) for providing the hydrometeorological data used in this study.

Conflicts of Interest: The authors declare no conflicts of interest.

References

1. IPCC. *Climate Change 2021: The Physical Science Basis*; Contribution of Working Group I to the Sixth Assessment Report of the Intergovernmental Panel on Climate Change; Cambridge University Press: Cambridge, UK, 2021. https://doi.org/10.1017/9781009157896.
2. IPCC. *Climate Change 2023: Synthesis Report*; Contribution of Working Groups I, II and III to the Sixth Assessment Report of the Intergovernmental Panel on Climate Change; Lee, H., Romero, J., Eds.; IPCC: Geneva, Switzerland, 2023; 184p. https://doi.org/10.59327/IPCC/AR6-9789291691647.
3. Trenberth, K.E. Changes in precipitation with climate change. *Clim. Res.* **2011**, *47*, 123–138. https://doi.org/10.3354/cr00953.
4. Donat, M.G.; Lowry, A.L.; Alexander, L.V.; O'Gorman, P.A.; Maher, N. More extreme precipitation in the world's dry and wet regions. *Nat. Clim. Change* **2016**, *6*, 508–513. https://doi.org/10.1038/nclimate2941.
5. WMO. *State of the Global Climate 2023*; WMO-No. 1347; World Meteorological Organization: Geneva, Switzerland, 2024. Available online: https://library.wmo.int/records/item/68835-state-of-the-global-climate-2023 (accessed on 2 January 2026).
6. Giorgi, F.; Lionello, P. Climate change projections for the Mediterranean region. *Glob. Planet. Change* **2008**, *63*, 90–104. https://doi.org/10.1016/j.gloplacha.2007.09.005.
7. Tramblay, Y.; Koutroulis, A.; Samaniego, L.; Vicente-Serrano, S.M.; Volaire, F.; Boone, A.; Le Page, M.; Llasat, M.C.; Albergel, C.; Burak, S.; et al. Challenges for drought assessment in the Mediterranean region under future climate scenarios. *Earth-Sci. Rev.* **2020**, *210*, 103348. https://doi.org/10.1016/j.earscirev.2020.103348.
8. Gudmundsson, L.; Boulange, J.; Do, H.X.; Gosling, S.N.; Grillakis, M.G.; Koutroulis, A.G.; Leonard, M.; Liu, J.; Müller Schmied, H.; Papadimitriou, L.; et al. Globally observed trends in mean and extreme river flow attributed to climate change. *Science* **2021**, *371*, 1159–1162. https://doi.org/10.1126/science.aba3996.
9. Knippertz, P.; Christoph, M.; Speth, P. Long-term precipitation variability in Morocco and the link to the large-scale circulation in recent and future climates. *Meteorol. Atmos. Phys.* **2003**, *83*, 67–88. https://doi.org/10.1007/s00703-002-0561-y.
10. Lionello, P.; Abrantes, F.; Congedi, L.; Dulac, F.; Gacic, M.; Gomis, D.; Goodess, C.; Hoff, H.; Kutiel, H.; Luterbacher, J.; et al. Introduction: Mediterranean Climate—Background Information. In *The Climate of the Mediterranean Region*; Lionello, P., Ed.; Elsevier: Oxford, UK, 2012; pp. xxxv–xc. https://doi.org/10.1016/B978-0-12-416042-2.00012-4.
11. Filahi, S.; Tanarhte, M.; Mouhir, L.; El Morhit, M.; Tramblay, Y. Trends in indices of daily temperature and precipitation extremes in Morocco. *Theor. Appl. Climatol.* **2015**, *124*, 959–972. https://doi.org/10.1007/s00704-015-1472-4.
12. Driouech, F.; Stafi, H.; Khouakhi, A.; Moutia, S.; Badi, W.; ElRhaz, K.; Chehbouni, A. Recent observed country-wide climate trends in Morocco. *Int. J. Climatol.* **2021**, *41*, E855–E874. https://doi.org/10.1002/joc.6734.
13. Verner, D.; Treguer, D.; Redwood, J.; Christensen, J.; McDonnell, R.; Elbert, C.; Konishi, Y.; Belghazi, S. *Climate Variability, Drought, and Drought Management in Morocco's Agricultural Sector*; World Bank Group: Washington, DC, USA, 2018. Available online: https://documents1.worldbank.org/curated/en/353801538414553978/pdf/130404-WPP159851-Morocco-WEB.pdf (accessed on 5 January 2026).
14. World Bank. *Morocco Country Climate and Development Report (CCDR)*; World Bank Group: Washington, DC, USA, 2022. https://doi.org/10.1596/38240.
15. Kessabi, R.; Hanchane, M.; Krakauer, N.Y.; Aboubi, I.; El Kassioui, J.; El Khazzan, B. Annual, seasonal, and monthly rainfall trend analysis through non-parametric tests in Sebou River Basin (SRB), Northern Morocco. *Climate* **2022**, *10*, 170. https://doi.org/10.3390/cli10110170.
16. ABHS. *Inventaire du Degré de Pollution des Ressources en Eau dans le Bassin du Sebou*; Agence du Bassin Hydraulique du Sebou: Fès, Morocco, 2015. Available online: https://www.abhsebou.ma/wp-content/uploads/2016/09/Inv_degre_pollution_2007.pdf (accessed on 2 January 2026).
17. Schilling, J.; Freier, K.P.; Hertig, E.; Scheffran, J. Climate change, vulnerability and adaptation in North Africa with focus on Morocco. *Agric. Ecosyst. Environ.* **2012**, *156*, 12–26. https://doi.org/10.1016/j.agee.2012.04.021.

18. El Moçayd, N.; Kang, S.; Eltahir, E.A.B. Climate change impacts on the Water Highway project in Morocco. *Hydrol. Earth Syst. Sci.* **2020**, *24*, 1467–1483. https://doi.org/10.5194/hess-24-1467-2020.
19. Perez Cutillas, P.; Salhi, A. Long-term hydroclimatic projections and climate change scenarios at regional scale in Morocco. *J. Environ. Manag.* **2024**, *371*, 123254. https://doi.org/10.1016/j.jenvman.2024.123254.
20. Chakri, A.; Laftouhi, N.-E.; Zouhri, L.; Ibouh, H.; Ibnoussina, M. Assessment of Satellite and Reanalysis Precipitation Data Using Statistical and Wavelet Analysis in Semi-Arid, Morocco. *Water* **2025**, *17*, 1714. https://doi.org/10.3390/w17111714.
21. Chakri, A.; Abakarim, S.; Rodrigues, J.C.A.; Laftouhi, N.-E.; Ibouh, H.; Zouhri, L.; Zaitseva, E. Spatial Bias Correction of ERA5_Ag Reanalysis Precipitation Using Machine Learning Models in Semi-Arid Region of Morocco. *Atmosphere* **2025**, *16*, 1234. https://doi.org/10.3390/atmos16111234.
22. Oukaddour, K.; Fakir, Y.; Le Page, M. Assessment of five global gridded precipitation estimates over a southern Mediterranean basin (Tensift, Morocco). *Geomat. Nat. Hazards Risk* **2025**, *16*, 2468850. https://doi.org/10.1080/19475705.2025.2468850.
23. Hersbach, H.; Bell, B.; Berrisford, P.; Hirahara, S.; Horányi, A.; Muñoz-Sabater, J.; Nicolas, J.; Peubey, C.; Radu, R.; Schepers, D.; et al. The ERA5 global reanalysis. *Q. J. R. Meteorol. Soc.* **2020**, *146*, 1999–2049. https://doi.org/10.1002/qj.3803.
24. Pettitt, A.N. A non-parametric approach to the change-point problem. *J. R. Stat. Soc. Ser. C (Appl. Stat.)* **1979**, *28*, 126–135. https://doi.org/10.2307/2346729.
25. Buishand, T.A. Some methods for testing the homogeneity of rainfall records. *J. Hydrol.* **1982**, *58*, 11–27. https://doi.org/10.1016/0022-1694(82)90066-X.
26. Ondo, J.-C.; Ouarda, T.B.M.J. Tests de Monte Carlo de détection de rupture(s)—Application à la détection d'un changement brusque du climat. *Rev. Afr. Rech. Inform. Math. Appl. (ARIMA)* **2025**, *43*, 13719. Available online: https://hal.science/hal-04588047v5/document (accessed on 7 January 2026).
27. Moriasi, D.N.; Arnold, J.G.; Van Liew, M.W.; Bingner, R.L.; Harmel, R.D.; Veith, T.L. Model evaluation guidelines for systematic quantification of accuracy in watershed simulations. *Trans. ASABE* **2007**, *50*, 885–900. https://doi.org/10.13031/2013.23153.
28. Teutschbein, C.; Seibert, J. Bias correction of regional climate model simulations for hydrological climate-change impact studies: Review and evaluation of different methods. *J. Hydrol.* **2012**, *456–457*, 12–29. https://doi.org/10.1016/j.jhydrol.2012.05.052.
29. Gudmundsson, L.; Bremnes, J.B.; Haugen, J.E.; Engen-Skaugen, T. Technical note: Downscaling RCM precipitation to the station scale using statistical transformations—A comparison of methods. *Hydrol. Earth Syst. Sci.* **2012**, *16*, 3383–3390. https://doi.org/10.5194/hess-16-3383-2012.
30. Cannon, A.J.; Sobie, S.R.; Murdock, T.Q. Bias correction of GCM precipitation by quantile mapping: How well do methods preserve changes in quantiles and extremes? *J. Clim.* **2015**, *28*, 6938–6959. https://doi.org/10.1175/JCLI-D-14-00754.1.
31. Boé, J.; Terray, L.; Habets, F.; Martin, E. Statistical and dynamical downscaling of the Seine basin climate for hydro-meteorological studies. *Int. J. Climatol.* **2007**, *27*, 1643–1655. https://doi.org/10.1002/joc.1602.
32. Giuntoli, I.; Renard, B.; Vidal, J.-P.; Bard, A. Low flows in France and their relationship to large-scale climate indices. *J. Hydrol.* **2013**, *482*, 105–118. https://doi.org/10.1016/j.jhydrol.2012.12.038.
33. Mann, H.B. Nonparametric tests against trend. *Econometrica* **1945**, *13*, 245–259. https://doi.org/10.2307/1907187.
34. Kendall, M.G. *Rank Correlation Methods*, 4th ed.; Charles Griffin: London, UK, 1975.
35. Sen, P.K. Estimates of the regression coefficient based on Kendall's tau. *J. Am. Stat. Assoc.* **1968**, *63*, 1379–1389. https://doi.org/10.2307/2285891.
36. McKee, T.B.; Doesken, N.J.; Kleist, J. The relationship of drought frequency and duration to time scales. In *Proceedings of the 8th Conference on Applied Climatology*; AMS: Anaheim, CA, USA, 1993; pp. 179–184.
37. Wang, G.; Jia, R.; Liu, J.; Zhang, H. Re-evaluation of the power of the Mann-Kendall test for detecting monotonic trends in hydrometeorological time series. *Front. Earth Sci.* **2020**, *8*, 14. https://doi.org/10.3389/feart.2020.00014.
38. Sebbar, A.; Badri, W.; Fougrach, H.; Hsaine, M.; Saloui, A. Étude de la variabilité du régime pluviométrique au Maroc septentrional (1935–2004). *Sécheresse* **2011**, *22*, 139–148.
39. Lionello, P.; Malanotte-Rizzoli, P.; Boscolo, R.; Alpert, P.; Artale, V.; Li, L.; Luterbacher, J.; May, W.; Trigo, R.; Tsimplis, M.; et al. The Mediterranean climate: An overview of the main characteristics and issues. *Dev. Earth Environ. Sci.* **2006**, *4*, 1–26. https://doi.org/10.1016/S1571-9197(06)80003-0.
40. Tarek, M.; Brissette, F.P.; Arsenault, R. Evaluation of the ERA5 reanalysis as a potential reference dataset for hydrological modelling over North America. *Hydrol. Earth Syst. Sci.* **2020**, *24*, 2527–2544. https://doi.org/10.5194/hess-24-2527-2020.
41. Jiang, Q.; Li, W.; Fan, Z.; He, X.; Sun, W.; Chen, S.; Wen, J.; Gao, J.; Wang, J. Evaluation of the ERA5 reanalysis precipitation dataset over Chinese Mainland. *J. Hydrol.* **2021**, *595*, 125660. https://doi.org/10.1016/j.jhydrol.2020.125660.

42. Sun, Q.; Miao, C.; Duan, Q.; Ashouri, H.; Sorooshian, S.; Hsu, K.L. A review of global precipitation data sets. *Rev. Geophys.* **2018**, *56*, 79–107. https://doi.org/10.1002/2017RG000574.
43. Beck, H.E.; Pan, M.; Roy, T.; Weedon, G.P.; Pappenberger, F.; Van Dijk, A.I.J.M.; Huffman, G.J.; Adler, R.F.; Ziegler, A.D. Daily evaluation of 26 precipitation datasets using Stage-IV gauge-radar data for the CONUS**.** *Hydrol. Earth Syst. Sci.* **2019**, *23*, 207–224. https://doi.org/10.5194/hess-23-207-2019.
44. Themeßl, M.J.; Gobiet, A.; Leuprecht, A. Empirical-statistical downscaling and error correction of daily precipitation from regional climate models. *Int. J. Climatol.* **2011**, *31*, 1530–1544. https://doi.org/10.1002/joc.2168.
45. Lafon, T.; Dadson, S.; Buys, G.; Prudhomme, C. Bias correction of daily precipitation simulated by a regional climate model: A comparison of methods. *Int. J. Climatol.* **2013**, *33*, 1367*–1381.* https://doi.org/10.1002/joc.3518.
46. Milly, P.C.D.; Betancourt, J.; Falkenmark, M.; Hirsch, R.M.; Kundzewicz, Z.W.; Lettenmaier, D.P.; Stouffer, R.J. Stationarity is dead: Whither water management? *Science* **2008**, *319*, 573–574. https://doi.org/10.1126/science.1151915.
47. Maraun, D.; Shepherd, T.G.; Widmann, M.; Zappa, G.; Walton, D.; Gutiérrez, J.M.; Hagemann, S.; Richter, I.; Soares, P.M.M.; Hall, A.; et al. Towards process-informed bias correction of climate change simulations. *Nat. Clim. Change* **2017**, *7*, 764–773. https://doi.org/10.1038/nclimate3418.
48. Vicente-Serrano, S.M.; Beguería, S.; López-Moreno, J.I. A multiscalar drought index sensitive to global warming: The SPEI. *J. Clim.* **2010**, *23*, 1696–1718. https://doi.org/10.1175/2009JCLI2909.1.